

# The impact of atmospheric stability and wind shear on vertical cloud overlap over the Tibetan Plateau

Jiming Li<sup>1,\*</sup>, Qiaoyi Lv<sup>2</sup>, Bida Jian<sup>1</sup>, Min Zhang<sup>1</sup>,  
Chuanfeng Zhao<sup>3</sup>, Qiang Fu<sup>1,4</sup>, and Kazuaki Kawamoto<sup>5</sup>, Hua Zhang<sup>6</sup>

5

<sup>1</sup>Key Laboratory for Semi-Arid Climate Change of the Ministry of Education, College of Atmospheric Sciences, Lanzhou University, Lanzhou, China

<sup>2</sup>Laboratory of Straits Meteorology, Xiamen Meteorological Bureau, Xiamen, China`

<sup>3</sup>State Key Laboratory of Earth Surface Processes and Resource Ecology, and College of Global Change and Earth System Science, Beijing Normal University, Beijing, China

<sup>4</sup>Department of Atmospheric Sciences, University of Washington, Seattle, USA

<sup>5</sup>Graduate School of Fisheries and Environmental Sciences, Nagasaki University, Nagasaki, Japan

<sup>6</sup>Laboratory for Climate Studies, National Climate Center, China Meteorological Administration, Beijing, China

15

Corresponding author: Jiming Li, Key Laboratory for Semi-Arid Climate Change of the Ministry of Education, College of Atmospheric Sciences, Lanzhou University, Lanzhou, Gansu 730000, China. ([lijiming@lzu.edu.cn](mailto:lijiming@lzu.edu.cn))

20

## Abstract

Studies have showed that the changes of cloud cover are responsible for the rapid climate warming over the Tibetan Plateau (TP) in the past three decades. To derive reliable simulation of the total cloud cover, atmospheric models have to reasonably represent the way of vertical overlap between cloud layers in them. Until now, however, this subject has received little attention due to the limited observation, especially over the TP. Based on the above information, the main aim of this study is to examine the cloud overlaps over the TP region, and build an empirical relationship between cloud overlap properties and large-scale atmospheric dynamics by using 4 years (2007–2010) of data from the CloudSat cloud product and collocated ERA-Interim reanalysis product. To do this, the cloud overlap parameter  $\alpha$ , which is an inverse exponential function of the cloud

30

layer separation  $D$  and decorrelation length scale  $L$ , is calculated and discussed. The parameter  $\alpha$  and  $L$  are both widely used to characterize the transition from the maximum to random overlap assumption with increasing layer separations. For those nonadjacent layers without clear sky between them (that is, contiguous cloud layers), it is found that the overlap parameter  $\alpha$  is sensitive to the unique thermo-dynamic and dynamic environment over the TP, i.e., the unstable atmospheric stratification and corresponding weak wind shear, which leads to maximum overlap (that is, greater  $\alpha$  values). This finding agrees well with the previous studies. Finally, we parameterize the decorrelation length scale  $L$  as a function of the wind shear and atmospheric stability based on a multiple linear regression. Compared with previous parameterizations, this new scheme can improve the simulation of total cloud cover over TP when the separations between cloud layers are greater than 1km. This study thus suggests that effects of both wind shear and atmospheric stability on cloud overlap should be taken into account in the parameterization of decorrelation length scale  $L$  in order to further improve the calculation of radiative budget and the prediction of climate change over TP in the atmospheric models.

50

55

60

## 1. Introduction

65 The Tibetan Plateau (TP), which is also known as the “roof of the world” or the  
“world water tower”, plays a significant role in determining global atmospheric  
circulations, in addition to its strong influence over Asia via its thermal-dynamic and  
dynamic forcings (Yanai et al., 1992; Ye and Wu, 1998; Duan and Wu, 2005; Xu et al.,  
2008; Wu et al., 2015). Some studies have showed that the TP has experienced significant  
70 climate warming over the past three decades (e.g., Yang et al., 2014; Kang et al., 2010),  
and it will continue in the future (e.g., Duan and Wu., 2006; Wang et al., 2008). The rapid  
warming has caused glacier retreat and expansion of glacier-fed lakes (Zhu et al., 2010),  
permafrost degradation (Cheng and Wu, 2007), and weakening of heating source (Yang et  
al., 2011). Based on the satellite and surface observations, many studies have linked the  
75 rapid warming over TP to the changes of cloud cover over this region (e.g., Chen and Liu,  
2005; Duan and Wu, 2006; Li et al., 2006; Yang et al., 2012; You et al., 2014). For  
example, a recent study has indicated that the increased nocturnal cloud cover over the  
northern TP could increase the nighttime temperature by enhancing downward surface  
infrared radiation, while the decreased daytime cloud cover over the southern TP has  
80 contributed to the increase of surface air temperature during daytime by enhancing  
downward surface solar radiation (Duan and Xiao, 2015). It means that the reliable  
simulation of cloud cover in the climate models will favor the prediction of climate  
change over TP.

However, our incomplete understanding of the cloud physical processes and the  
85 limited cloud observations over the TP make the simulation of total cloud cover in the  
climate models still unreliable. One of the remaining challenges involves how to  
reasonably represent the characteristics of the vertical overlapping of cloud layers in  
these models. Cloud overlap means that two or more cloud layers are simultaneously  
present over the same location but at different levels in the atmosphere. To derive the  
90 reasonable total cloud cover between cloud layers, models have to make some  
assumption about the cloud layers how to overlap in the vertical direction, such as,  
maximum, random and minimum assumptions. If the cloud covers of two model layers  
are given by  $C_i$  and  $C_j$ , respectively, total cloud cover between these two layers from  
maximum assumption is  $C_{i,j}^{\max} = \max\{C_i, C_j\}$ , while the random and minimum

95 assumptions define the total cloud cover as  $C_{i,j}^{ran} = C_i + C_j - C_i \times C_j$  and  
 $C_{i,j}^{min} = \min\{C_i + C_j, 1\}$ , respectively. Thus, the maximum assumption minimizes the total  
cloud cover, while minimum assumption produces minimally overlap between cloud  
layers and results in maximum total cloud cover (Weger et al., 1992). The total cloud  
cover predicted by the random assumption will fall somewhere between maximum and  
100 minimum assumption (Geleyn and Hollingsworth, 1979). Studies have shown that these  
different overlap assumptions result in obvious different total cloud covers and will  
significantly affect the calculated radiative budgets and heating/cooling rate profiles  
(Morcrette and Fouquart, 1986; Barker et al., 1999; Barker and Fu, 2000; Chen et al.,  
2000; Pincus et al., 2005; Zhang and Jing, 2010; 2016; Zhang et al., 2013; Jing et al.,  
105 2016).

To improve the simulation of total cloud cover, Hogan and Illingworth (2000)  
revisited the cloud overlap assumptions and proposed a simpler and more useful  
expression for the degree of cloud layer overlap (exponential random overlap assumption)  
by using the ground-based radar measurement. In the expression, the observed cloud  
110 cover between two cloud layers can be expressed as the linear combination of the  
maximum and random overlap by using a weighting factor, termed as cloud overlap  
parameter  $\alpha$  :

$$\alpha = \frac{C_{i,j}^{obs} - C_{i,j}^{ran}}{C_{i,j}^{max} - C_{i,j}^{ran}} \quad (1)$$

The overlap parameter  $\alpha$  ranges from 0 (random) to 1 (maximum) when the observed  
115 total cloud cover falls between the values using the maximum and random overlap  
assumptions. The  $\alpha$  will be negative if the degree of cloud overlap is lower than that  
predicted by the random overlap assumption. Finally, Hogan and Illingworth (2000) fitted  
the reduction in  $\alpha$  with layer separation  $D$  as an inverse exponential function of the  
decorrelation length scale  $L$ :  $\alpha = e^{-D/L}$ . Thus,  $\alpha$  and  $L$  are both used to characterize the  
120 transition from the maximum to random overlap assumption with increasing layer  
separations. Until now, many efforts have been made to derive the values of  $\alpha$  and  $L$   
using ground-based radar observations (e.g. Mace and Benson-Troth, 2002; Willén et al.,  
2005; Naud et al., 2008; Oreopoulos and Norris, 2011) and improve the representation of

$L$  in the models (Shonk et al 2010; 2014; Di Giuseppe and Tompkins, 2015). For example,  
125 Oreopoulos and Norris (2011) derived  $L$  based on radar measurement taken over the US  
Southern Great Plains (SGP). Their results indicated that  $L$  ranges from 2 to 4.5 km  
across different seasons and smaller spatial scales correspond with smaller  $L$  values.  
Based on two months of cloud mask profile information from the Space-based radar and  
lidar, Barker (2008) quantified the properties of cloud overlap on a global scale and found  
130 a wide range of  $L$  values, with a median value of 2 km. In other studies, decorrelation  
length scale  $L$  is also parameterized as a function of latitude (Shonk et al., 2010; 2014),  
total cloud cover (Yoo et al., 2014) or wind shear (Di Giuseppe and Tompkins, 2015).  
These findings suggest that meteorological factors could be connected to the overlap way  
between cloud layers.

135 To date, however, the related question of the cloud overlapping over the TP region  
has received little attention due to the limited observation. It is still an open question on  
how the unique thermo-dynamic and dynamic environment over the TP region affects  
cloud overlap there. The millimeter-wavelength cloud profiling radar (CPR) launched on  
CloudSat (Stephens et al., 2002) and the cloud-aerosol lidar with orthogonal polarization  
140 (CALIOP) (Winker et al., 2007) launched on CALIPSO (Cloud-Aerosol Lidar and  
Infrared Pathfinder Satellite Observation) provide an unprecedented opportunity to  
investigate vertical cloud overlaps on a global scale (e.g., Barker et al., 2008; Kato et al.,  
2010; Mace et al., 2009; Li et al., 2011; 2015; Tompkins and Di Giuseppe, 2015). In the  
following study, we investigate the cloud overlap properties over the TP region and  
145 identify an empirical relationship between decorrelation length scale  $L$  and large-scale  
atmospheric dynamics by combining the cloud cover profile information from the  
2B-GEOPROF-LIDAR dataset (Mace et al., 2009; Mace and Zhang, 2014) and the  
meteorological fields from the ERA-Interim reanalysis datasets (Dee et al., 2011). The  
parameterization of decorrelation length scale  $L$  will favor the simulation of total cloud  
150 cover and the calculation of radiative energy budget over TP in the models. This paper is  
organized as follows. The datasets and methods used in this study are briefly described in  
Section 2. Section 3 outlines the monthly and zonal variations of the cloud overlap  
parameters over the TP region. The impacts of the atmospheric state and large-scale  
atmospheric dynamics on cloud overlap are presented in Sections 4. The conclusions and

155 discussion are given in Section 5.

## 2. Datasets and methods

4 years (2007–2010) of data from the CloudSat 2B-GEOPROF-LIDAR, ECMWF-AUX and the daily 6-hour ERA-Interim reanalysis are used to analyze the impacts of atmospheric states and dynamics on the cloud overlap over the TP  
160 (27°N–39°N; 78°E–103°E) region ( Fig. 1a).

### 2.1 Satellite datasets

Radar signals can penetrate the optically thick cloud layers that attenuate lidar signals, but lidar signals may sense the optically thin hydrometeor layers that are below the detection threshold of radar signals. Thus, with the unique complementary capabilities of  
165 the CPR on CloudSat and the CALIOP on the CALIPSO, the 2B-GEOPROF-LIDAR dataset produces the most accurate description of the locations of the hydrometeor layers in the atmosphere on the global scale (Mace and Zhang, 2014). In this dataset, every CloudSat profile includes 125 height layers (e.g., vertical bin), and the “*Cloud Fraction*” parameter reports the fraction of the lidar volume within each radar vertical bin that  
170 contains hydrometeors (Mace et al., 2009; Mace and Zhang, 2014). Several previous studies have identified a cloudy atmospheric bin based on different thresholds of the lidar-identified cloud fraction, including a 99% (Barker, 2008; Di Giuseppe and Tompkins, 2015) or a 50% threshold (Haladay and Stephens, 2009; Verlinden et al., 2011). Here, a threshold of 99% is used in our study. Due to the significant attenuation of lidar  
175 signals to the optically thick layers, this parameter fails to provide the “*Cloud Fraction*” for optically thick layers. Thus, we also use the radar information (i.e., cloud “*LayerBase*” and “*LayerTop*” fields) from the aforementioned dataset to construct the complete two-dimensional cloud mask (See Fig. 1b). It is noting that the 2B-GEOPROF-LIDAR dataset does not distinguish cloud and precipitation, therefore any bias in our results  
180 caused by precipitation can't be removed in current analysis. Besides the 2B-GEOPROF-LIDAR dataset, the ECMWF-AUX dataset (Partain, 2004), which is an intermediate dataset that are the ancillary ECMWF state variables interpolated across each CloudSat CPR bin, is also used to provide the pressure and height information of each vertical bin in the cloud mask profile. The vertical and horizontal resolutions of  
185 these products are 240 m and 1.1 km, respectively. To avoid sunlight scattering

contamination to lidar observation and minimize surface contamination of the CPR, we only use the nighttime datasets above 1 km over the TP surface in the following analysis.

## 2.2 Meteorological reanalysis dataset

The 6-hourly ERA-Interim reanalysis with a grid resolution of  $0.25^\circ \times 0.25^\circ$  (Dee et al., 2011), is used to characterize the atmospheric thermodynamic and dynamic states over the TP. For each cloud mask profile in the 2B-GEOPROF-LIDAR, the vertical profiles of the zonal wind  $u$ , meridional wind  $v$ , relative humidity  $rh$ , specific humidity  $sh$  and atmospheric temperature  $T$  closest to the cloud profile in both space and time are extracted and further interpolated vertically to match the vertical bins of the cloud mask profile. Following Di Giuseppe and Tompkins (2015), the  $u$  and  $v$  winds at every vertical bin are then projected onto the satellite overpass track, being averaged in the along-track direction for all profiles in the selected CloudSat data segment to derive the scene-average, along-track horizontal wind  $V$ . Here, we define the wind shear  $dV/dz_{i,j}$  between the layers  $i$  and  $j$ , as follows:

$$dV/dz_{i,j} = \frac{\max\{V_i; V_j\} - \min\{V_i; V_j\}}{D_{i,j}}, \quad (2)$$

Where  $V_i$  and  $V_j$  are the horizontal winds at layers  $i$  and  $j$ , respectively, and  $D_{i,j}$  is the layer separation distance. The derived wind shear will be used to calculate the cloud overlap parameter. For the CloudSat overpass track (Fig. 1a), Di Giuseppe and Tompkins (2015) indicated that the cross-track shear of the zonal wind  $u$  has little statistical significance.

Similarly to the wind shear, we calculate the vertical gradient of the saturated equivalent potential temperature ( $\partial\theta_{es}/\partial z_{i,j}$ ) between the same two layers to quantify the dependence of the cloud overlap on the degree of the conditional instability of the moist convection. Here,

$$\begin{aligned} \theta_{es} &= \theta \exp\left(\frac{L_v r_s}{C_p T}\right) \\ \theta &= T \left(\frac{1000}{p}\right)^{0.286}, L_v = 2.5 \times 10^6 - 2323 \times (T - 273.16) \\ r_{s=} &= \frac{sh}{rh \times (1 - sh)} \end{aligned} \quad (3)$$

where  $\theta$  is the potential temperature,  $L_v$  is the latent heat of vaporization,  $r_s$  is the

saturation mixing ratio,  $C_p$  is the specific heat capacity at a constant pressure, and  $T$  is the atmospheric temperature. The smaller the  $\partial\theta_{es}/\partial z_{i,j}$ , the more unstable the atmosphere. Furthermore, the scene-averaged vertical velocity at 500 hPa is also extracted from the ERA-Interim reanalysis to analyze the impact of vertical motion on cloud overlap. The positive values are for the updraft, and negative values are for the subsidence.

### 2.3 The overlap parameter and its dependence on the spatial scale

Previous studies have shown that the overlap parameter  $\alpha$  and decorrelation length  $L$  are sensitive to the spatial scale of the GCM's grid box (Hogan and Illingworth, 2000; Oreopoulos and Khairoutdinov, 2003; Oreopoulos and Norris, 2011; Pincus et al., 2005). For example, Hogan and Illingworth (2000) found that cloud overlap parameter tends to increase with decreasing spatial and temporal resolutions (i.e., increasing vertical and horizontal grid scales) of GCMs.

To examine the dependence of overlap parameter on the spatial scale, each CloudSat orbit over the TP region is divided into segments with different horizontal lengths including 25, 50, 100 and 200 km. Hereafter, this horizontal length is referred to as the spatial scale of the GCM's grid box. Fig.1b shows an example of cloud mask from the 2B-GEOPROF-lidar dataset over the TP region. This cloud mask includes eight, four, two and one segments, which correspond to the horizontal resolution of 25, 50, 100 and 200 km, respectively. Given the threshold of 99% for cloud fraction, the segment-average cloud cover profile of each segment is first derived. Here, it is important to emphasize that cloud fraction and cloud cover are different variables in our study. The “*Cloud fraction*” reports the fraction of lidar volumes in each radar vertical bin that contains hydrometeors and is used to identify a cloudy atmospheric bin based on the chosen threshold, which is 99% in this study. When averaging all cloud fraction profiles in the along-track direction for given CloudSat data segment, we derive the segment-average cloud cover profile, which represents the percentage of clouds in a given spatial scale and certain height. Then, the vertical overlap between any two atmospheric layers in this profile is calculated if the cloud covers ( $C_i$  and  $C_j$ ) of both layers exceed 0. Layers are analyzed in pairs and no ‘double-counting’. If cloud layer pairs have the same separation distance but different altitudes, they will be categorized into the same statistic group. Following Hogan and Illingworth (2000) and Di Giuseppe and Tompkins (2015), we



consider the nonadjacent layers to be a contiguous cloud pair when all layers between them are classified as cloud layers. Otherwise, these layers are classified as a noncontiguous cloud pair (Hogan and Illingworth, 2000; Di Giuseppe and Tompkins, 245 2015).

Based on the definitions of different overlap assumptions and  $\alpha$  in the introduction section, Figs.1c and 1d show an example of the observed and calculated segment-average cloud cover profiles based on maximum and random assumptions, and corresponding overlap parameters of contiguous cloud pairs for 25, 50, 100 and 200 km spatial scale in given cloud mask sample (Fig. 1b). It is clear that the observed and calculated cloud 250 covers and corresponding overlap parameters tend to increase as the spatial scale increases. Meantime, the observed cloud covers tend to transform from the maximum to random overlap assumption with increasing layer separations.

By collecting 4 years of cloud sample from the 2B-GEOPROF-LIDAR dataset, 255 Figs.2a and 2b further show the dependence of  $\alpha$  on the layer separation and its sensitivity to the spatial scale for both noncontiguous and contiguous cloud layers. Many studies have used ground- and space-based radars to examine the validity of the random overlap assumption for the vertically noncontiguous clouds (Hogan and Illingworth, 2000; Mace et al., 2002; Naud et al., 2008; Di Giuseppe and Tompkins, 2015). Fig.2a shows 260 that the degree of cloud overlap of the noncontiguous clouds over the TP region is lower than the random overlap, especially when the layer separation is smaller than 2km. Given the spatial scale of 50 km, almost all of the  $\alpha$ -values are negative and fall between -0.25 and -0.05. Thus, the total cloud cover would still slightly be underestimated for noncontiguous cloud pairs by using the random overlap assumption. Assuming a cloud 265 layer separation of less than 9 km,  $\alpha$  for noncontiguous cloud pairs increases as the spatial scale increases (e.g., from 25 km to 200 km). For a contiguous cloud pair (Fig. 2b),  $\alpha$  decrease from 0.95 to 0 with an increasing separation. Meantime, a slight dependence of  $\alpha$  on the spatial scale is also observed for contiguous cloud pairs when they are separated by a distance of about 1 km to 4 km. This indicates that the maximum overlap 270 is slightly more common for a larger horizontal domain, which is consistent with previous studies (Hogan and Illingworth, 2000; Oreopoulos and Khairoutdinov, 2003; Oreopoulos and Norris, 2011).

## 2.4 Selection of thresholds for cloud cover and spatial scale

About the dependence of  $\alpha$  on the spatial scale, Tompkins and Di Giuseppe (2015) theorized that some overcast or single cloud layers would be removed from the samples when the spatial scale is smaller than the cloud system scale, thus biasing  $\alpha$  and its decorrelation length  $L$ . Given a spatial scale of 50 km, the ratio of the spatial scale to the cloud system scale decreases strongly from the equator to the poles because many of the frontal cloud systems of the middle and high latitudes are larger than the convective cloud systems over the tropics. Ultimately, the corresponding bias in  $\alpha$  would increase with latitude. For the foregoing reasons, regional atmospheric models should account for the typical cloud system scale in their parameterization schemes when using a fixed horizontal resolution.

Fig. 2c depicts the probability distribution functions (PDFs) of the horizontal scales of the along-track cloud systems at different heights over the TP region. Here, the horizontal scale of a cloud system at a given height along the CALIPSO/CloudSat track is determined by calculating the number of continuous cloud profiles ( $N$ ) at a given height. Using a 1.1 km along-track resolution for the CPR measurements, the along-track scale ( $S$ ) of a cloud system is  $S=N \times 1.1$  km (Zhang et al., 2014; Li et al., 2015). It is clear that the probability of cloud system with small-scale decreases with increasing height (Fig.2c). The mean horizontal scale of 59.2 km for a cloud system at a height of 15 km is almost twelve times greater than that (i.e., 4.6 km) at a height of 2 km. For TP region, we can see that the horizontal scales of cloud system below 10 km are smaller than the spatial scale of 50 km, thus we apply the spatial scale of 50 km to perform the following analysis although this scale would still result in significant errors in  $\alpha$  at higher atmospheric heights (e.g., 15km) where cloud has large horizontal scale.

In addition, to further reduce the sensitivity of  $\alpha$  to the spatial scale caused by data truncation, we follow the study from Tompkins and Di Giuseppe (2015) and apply a simple data filter so that only atmospheric layers with segment-average cloud cover below a given threshold of 50% are retained. As stated by Tompkins and Di Giuseppe (2015), data might still be truncated with this filter, but the sensitivity of the results to the spatial scale should largely be reduced. After limiting the spatial scale (50 km) and upper limit of cloud cover (50%), the number of available cloud layer-pair samples is still at

least one million, thus ensuring statistical significance. Fig.2d shows the variations of  
305 sample number and the cumulative percentage with cloud layer separation for both  
noncontiguous and contiguous clouds at a given spatial scale of 50 km. It shows that the  
cumulative proportion of cloud sample significantly increases with increasing layer  
separation. For the contiguous cloud, the cumulative percentage accounts for 90% of all  
samples when layer separation is smaller than 4 km. Given the 1.1 km along-track  
310 resolution of the CPR measurements and a spatial scale of 50 km (that is, about 50  
CloudSat profiles), the each cloudy CloudSat profile has a cloud cover about 2% (Di  
Giuseppe and Tompkins, 2015).

### 3. Monthly and zonal variations of overlap parameter for contiguous clouds

Figure 3a shows the monthly variations in  $\alpha$  for the contiguous cloud-pairs based  
315 on pentad-average over the TP. In Fig.3a, the maximum separation of contiguous cloud  
layers gradually increases from January (approximately 6 km) to August (beyond 8 km)  
and then gradually decreases, indicating that the cloud systems over TP during summer  
are thicker than other seasons due to frequent strong convective motions. When the cloud  
layer separation is less than 1 km, the overlap parameter  $\alpha$  has little monthly variation and  
320 is always large (even beyond 0.7). However, the monthly variation of  $\alpha$  becomes  
manifest as the layer separation is larger than 1 km. For a 2-km cloud separation, e.g.,  $\alpha$   
reaches its maximum of 0.45 in August and a minimum of 0.1 in February (see Fig. 3d).  
For a separation of 3 km,  $\alpha$  is generally lower but has the similar monthly variation to  
those seen for a 2-km separation. By checking the negative value of  $\alpha$  in Fig.3a, it is  
325 clear that even random overlap assumption could underestimate the total cloud cover  
between two cloud layers with large separation during all seasons except summer. These  
cloud overlap features may be associated with the unique topographical forcing and  
corresponding thermo-dynamic and dynamic environment of the TP. In summer, the TP is  
usually considered as an atmospheric heat source or “air pump” due to its higher surface  
330 temperature compared with surrounding regions at the same altitude (Wu et al., 2015).  
Additionally, a humid and warm air intrudes from the South Asia monsoon area into the  
lower atmosphere over the TP would intensify the atmospheric instability of moist  
convection when combined with the enhanced surface heating (Taniguchi and Koike,  
2008). This process further promotes the transportation of water vapor into high altitudes

335 and favors the development of convective clouds. Indeed, satellite observations have indicated that cumulus prevails over the TP during the summer (Wang et al., 2014; Li and Zhang, 2016).

Due to cumulus over the TP has a small horizontal scale, thus a 50 km-spatial scale from CloudSat should not bias  $\alpha$  estimate too much in our study. However, previous  
340 studies have pointed out that precipitation may bias the cloud overlap statistics toward maximum overlap (Mace et al., 2009; Di Giuseppe and Tompkins, 2015). Present study does not eliminate the influence of precipitation on the overlap parameter. If we exclude the samples with precipitation from the analysis, the overlap parameter  $\alpha$  would become smaller. The feature may be even more obvious during summer due to more frequent  
345 precipitation over TP during this season (Yan et al., 2016). The seasonal variation of  $\alpha$  is also found at different ground sites (Mace and Benson-Troth, 2002; Naud et al., 2008). For example, Oreopoulos and Norris (2011) indicated that clouds tend to be more random in the winter and most maximum during the summer. In fact, these overlap properties are associated with cloud system scale, which is dominated by dynamical situation  
350 (Tompkins and Di Giuseppe, 2015).

Figures 3b and 3c show the monthly variations in pentad-averaged conditional instability of the moisture convection ( $\partial\theta_{es}/\partial z$ ) and the wind shear ( $dV/dz$ ) for the contiguous cloud-pairs over the TP, respectively. The  $\partial\theta_{es}/\partial z$  and  $dV/dz$  both exhibit obvious monthly variations for all cloud-layer separations. The atmospheric stability and  
355 wind shear gradually decrease from January to August and then steadily increase (see Figs. 3c, 3d, 3e and 3f). From Fig.3c, we can see that the adjacent atmospheric layers during May to September tend to be more unstable and have weak wind shear. These atmospheric states favor the development of clouds and result in maximum overlap between cloud layers. During other month (e.g., December), clouds also tend to follow  
360 the maximum overlap more although adjacent atmospheric layers are stable with large  $\partial\theta_{es}/\partial z$  and  $dV/dz$ . It might be the case that vertical velocities might be large because of extratropical cyclones or other baroclinic instability. With the layer separation increases, atmospheric layers become more stable and then favor random overlap, especially during summer season. These results verify that a more unstable atmosphere

365 tends to favor a maximum overlap over a random one, as shown in previous studies  
(Mace and Benson-Troth, 2002; Naud et al., 2008). Note that Figs. 3d and 3f might reveal  
an inconsistency between the wind shear and atmospheric stability. For example, we can  
see that the wind shear for a 2-km layer distance is greater than that for a 3-km distance,  
but the atmosphere is also more unstable. This inconsistency is probably because two  
370 cloud layers with the same separation but at different altitudes are sorted into the same  
statistical group. Or, it is also quite possible that other large scale forcings might  
influence the overlap. In addition, we find the monthly variations in pentad-averaged  
vertical velocity ( $\omega$ ) at 500 hPa (see Figs.3g and 3h) are also consistent with the monthly  
cycle of  $\alpha$ . It means that vigorous ascent tends to favor maximum overlap. This result  
375 agrees well with the previous studies (Naud et al., 2008).

Figure 4 shows the zonal variations of  $\alpha$ ,  $\partial\theta_{es}/\partial z$ ,  $dV/dz$  and  $\omega$  over the TP. Figs.  
4a and 4b indicate that  $\alpha$  is larger in the south part of the TP and smaller in the north.  
This is mainly because the atmospheric instability in the southern part of the TP enhances  
the convective activity (Fujinami and Yasunari, 2001). Due to the weakening of the  
380 monsoon and the blocking by topography, less water vapor may reach the northern part,  
and thus fewer clouds from there (You et al., 2014). Compared with the southern TP, the  
stability and wind shear are both larger over the northern part, especially for those cloud  
layers with large separation (e.g., >2km). This meteorological condition will result in  
more frequent negative  $\alpha$ , indicating that random overlap assumption used in models  
385 would underestimate the total cloud cover and thus bias the surface radiation over these  
regions (see Fig.4a). The most significant warming occurring over the northern part of TP  
has been attributed to pronounced stratospheric ozone depletion (e.g., Guo and Wang,  
2012). However, a more recent study indicates that the accelerated warming trend over  
the Tibetan Plateau may be due to the rapid cloud cover increases at nighttime over the  
390 northern Tibetan Plateau and the sunshine duration increase in the daytime over the  
southern Tibetan Plateau (Duan and Xiao, 2015). Therefore, an accurate representation of  
cloud overlap and its relations to atmospheric thermodynamic and dynamic conditions in  
models is critically important to the understanding of rapid warming over the TP.  
Although it is still difficult for models to capture the cloud overlap properties, especially  
395 for those cloud layers with large separation over north TP, our results confirm that the  $\alpha$

is well related with wind shear and instability. However, the zonal variation of  $\alpha$  is inconsistent with the variation of vertical velocity (see Figs. 4g and 4h).

#### 4. Sensitivity of $\alpha$ on the meteorological conditions and its parameterization

To facilitate the parameterization of  $\alpha$  for cases of contiguous clouds, we further  
400 investigate the sensitivity of  $\alpha$  on the different meteorological conditions. Here, each meteorological factor over the TP region is grouped into one of four bins as follows. The four bins for  $\partial\theta_{es}/\partial z$  are  $\partial\theta_{es}/\partial z > 5$  K/km,  $2.5 < \partial\theta_{es}/\partial z < 5$  K/km,  $0 < \partial\theta_{es}/\partial z < 2.5$  K/km and  $\partial\theta_{es}/\partial z < 0$  K/km. For wind shear, the four bins are  $dV/dz < 0.5$  m  $\cdot$  s<sup>-1</sup>/km,  $0.5 < dV/dz < 2$  m  $\cdot$  s<sup>-1</sup>/km,  $2 < dV/dz < 3.5$  m  $\cdot$  s<sup>-1</sup>/km and  $dV/dz > 3.5$  m  $\cdot$  s<sup>-1</sup>/km. For  
405 vertical velocity, the four bins are  $\omega < -40$  hPa/day,  $-40 < \omega < 0$  hPa/day,  $0 < \omega < 40$  hPa/day and  $\omega > 40$  hPa/day. These groupings ensure that a statistically significant number of samples fall within each bin (i.e., at least one hundred thousand samples per bin). In addition, Li et al. (2015) indicated that the overlap properties between different cloud types are obvious different but the most significant components of the global  
410 climate system. Although current study doesn't include the information of cloud type, the sensitivity of  $\alpha$  on the meteorological parameters in our analysis actually exhibit the effects of cloud types on the  $\alpha$  due to different combinations of cloud type with same layer separation possibly take place in distinct wind shear and stability conditions.

Figure5 illustrates the sensitivity of  $\alpha$  to wind shear, instability and vertical velocity  
415 at given upper limit of cloud cover (50%) and spatial scale (50 km) for the contiguous clouds. Since the cloud samples with layer separation below 3.5 km account for 90% of all samples for contiguous clouds, we only present the results for layer distances smaller than 3.5 km. Naud et al. (2008) tested the sensitivity of  $\alpha$  to wind shear at three sites and found that wind shear slightly affects  $\alpha$  when the layer distance is larger than 2 km. In a  
420 recent study, Di Giuseppe and Tompkins (2015) demonstrated the important effect of wind shear on the global cloud overlap by using a combination of the CloudSat-CALIPSO cloud data and the ECMWF reanalysis dataset. Our results along with previous studies suggest that the cloud overlap strongly depends on atmospheric conditions, but their relationship displays some variability, in particular spatially and  
425 seasonally. The effect of the atmospheric stability on cloud overlap may be more

important over convective regions (e.g., the intertropical convergence zone and TP during summer season) while the effect of wind shear may be dominant over the mid-latitudes. Besides the wind shear and instability, some studies also tested the sensitivity of the overlap parameter to the large-scale vertical velocity. For example, Naud et al. (2008) indicated that vertical velocities in the tropics are not captured in the reanalysis dataset when convection occurs, thus they only discussed the impact of vertical velocity on the cloud overlap parameter over the mid-latitude and found that vigorous ascent tends to favor maximum overlap. Fig.5c shows that vertical velocity at 500hPa has somewhat effect to cloud overlap parameter. However, by combining the effects of wind shear, instability and vertical velocity into parameterization of decorrelation length scale  $L$ , we find that this scheme doesn't show better superiority than the scheme which only includes the wind shear and instability.

Here, we derive the decorrelation length scale  $L$  values (km) from the least squares exponential fit to the original  $\alpha$  curve at given wind shear and instability bin. Then, we further parameterize  $L$  as a function of wind shear or both wind shear and atmospheric instability based on a (multiple) linear regression. The regression formula of  $L$  can be written as:

$$L = L_{\alpha} - b1 \frac{\partial \theta_{es}}{dz} - b2 \frac{dV}{dz}$$

*or*

$$L = L_{\alpha1} - c1 \frac{dV}{dz}$$
(4)

Here,  $L_{\alpha}$ ,  $L_{\alpha1}$ ,  $b1$ ,  $b2$ , and  $c1$  are the fitting parameters. Table 1 lists several parameterization schemes for the decorrelation length scale  $L$ . The scheme with wind shear from Di Giuseppe and Tompkins (2015) using the global CloudSat-CALIPSO cloud data and ECMWF reanalysis dataset is shown for a comparison. Di Giuseppe and Tompkins (2015) discussed the uncertainties from fitting methods and calculation of wind shear. Related to the observational orbit, the impact of cross-track wind shear is neglected in our study, which would exclude many large wind shears associated with jet structures (Di Giuseppe and Tompkins, 2015). The parameterization scheme of Shonk et al. (2010) is also shown in Table 1, which is an empirical linear relationship between  $L$  and latitude based on CloudSat and CALIPSO data. Our parameterization schemes in terms of wind

shear or both wind shear and instability are given in Table 1. Note that the R-squared  
455 values ( $R^2$ ) for our wind shear and wind shear-instability schemes are 0.88 and 0.96,  
respectively.

After deriving the regression formula of decorrelation length scale  $L$ , we re-apply it  
to all contiguous cloud samples and retrieve the  $L$  and corresponding  $\alpha$  based on the  
formula:  $\alpha = e^{-D/L}$  and dynamical conditions. Finally, retrieved overlap parameter  $\alpha$  is  
460 used to calculate the total cloud cover between any two cloud layers by using the Equ. (1)  
and the definitions of random and maximum overlap assumptions. Figure 6 presents the  
monthly difference between calculated and observed cloud covers using various overlap  
parameterization schemes. It is seen that the maximum and random overlap assumptions  
result in large cloud cover biases, especially for layer separations greater than 1 km for  
465 maximum overlap and less than 2 km for random overlap where the bias exceeds 5%.  
Compared with random and maximum assumptions, the differences of total cloud over  
caused by other schemes are small and range from -3% to 3%. In addition, the wind shear  
scheme and the wind shear-instability scheme from the present study overall show less  
biases than other schemes. However, several points still need to be further noticed. First,  
470 the wind shear scheme from Di Giuseppe and Tompkins (2015) significantly  
underestimates the cloud cover for layer separations above 1 km (e.g., reach 3%). This  
large bias may be because it is based on the global CloudSat-CALIPSO measurements  
and ECMWF reanalysis dataset for a short period (January-July 2008); as such, some  
obvious regional or seasonal cloud overlap properties are easily obscured by global  
475 averaging. Furthermore, the role of atmospheric stability is not considered in this scheme.  
However, the scheme from Di Giuseppe and Tompkins (2015) causes little bias for layer  
separations below 1 km. This is because this scheme retrieves much larger  $L$  and overlap  
parameter values than other schemes. An interesting finding is that Shonk/latitude  
scheme leads to comparable bias with new schemes from this study. The bias is even  
480 smaller for Shonk/latitude scheme when the layer separation is below 1 km. In fact, Fig.5  
has demonstrated that the sensitivity of  $\alpha$  to wind shear and instability is rather weak  
when cloud layers are very close. Compared with our wind shear scheme, our wind  
shear-instability scheme further combines the impact of atmospheric instability and has a  
relatively lower bias at large layer separations with higher R-squared values ( $R^2=0.96$ ).



485 Fig.7 shows the zonal difference between calculated and observed cloud covers for  
the aforementioned schemes. The differences of cloud cover caused by different overlap  
schemes are distinguishable. Similar with Fig.6, the maximum and random overlap  
assumptions still result in the most prominent cloud cover biases (exceed  $\pm 5\%$ ) at most  
of the layer separations. Compared with our wind shear scheme and wind  
490 shear-instability schemes, the scheme from Di Giuseppe and Tompkins (2015) and  
latitude scheme from Shonk et al. (2010) cause relatively obvious underestimation of  
total cloud cover when cloud layer separations exceed 1 km, especially for scheme from  
Di Giuseppe and Tompkins (2015) (bias reach -3%). Only if cloud layer separations are  
smaller than 1 km, these two schemes produce better cloud cover simulation than our  
495 schemes. In summary, these results indicate that new parameterization (that is, our wind  
shear-instability scheme) of decorrelation length scale  $L$ , which includes the effects of  
both wind shear and atmospheric stability on cloud overlap, may improve the simulation  
of total cloud cover over TP.

## 5. Conclusions and discussion

500 Clouds strongly modulate the Earth's radiative energy budget via changes in their  
macro- and micro-physical properties (e.g., Hartmann et al., 1992; Fu and Liou, 1993; Fu  
et al., 2002; Kawamoto and Suzuki, 2012; Yan et al., 2012; Wang et al., 2010). Many  
studies have showed that annual and seasonal changes of total cloud cover are responsible  
for the rapid climate warming over the Tibetan Plateau in the past three decades (e.g.,  
505 Yang et al., 2012; You et al., 2014; Duan and Xiao, 2015).

To accurately simulate the total cloud cover and its impact on the radiative energy  
budget, climate models need to reliably represent the cloud vertical overlap, which has  
received less attention than necessary because of the limited regional cloud observations.  
In view of the passive sensors only provide limited information about the cloud overlap  
510 (Chang and Li, 2005a, b; Huang, 2006; Huang et al., 2005, 2006a) and the vertically  
resolved advantage of active sensors (Ge et al., 2017; 2018), this study utilizes the 4 years  
(2007–2010) of data from the space-based radar cloud product and collocated  
ERA-Interim reanalysis product to analyze the cloud overlaps over the Tibetan Plateau  
and build an empirical relationship between cloud overlap properties and large-scale  
515 atmospheric dynamics. It is confirmed that the contiguous cloud layers tend to have

maximum overlap at small separation but gradually become randomly overlapped with an increase of the layer separation. Focusing on the contiguous cloud layers, we evaluate the effects of the meteorological conditions on the cloud overlap. It is found that the unstable atmospheric stratification with a weak wind shear over the TP would tend to favor maximum overlap, agreeing well with previous studies. We parameterize the decorrelation length scale  $L$ , which is used to characterize the transition from the maximum to random overlap assumption, as a function of the wind shear and atmospheric stability. Compared with other parameterizations, this new scheme improves the prediction of total cloud cover over TP when cloud layers separations are greater than 1km. Although the scheme derived in our study focuses only on the TP, our results suggest that the parameterization of the decorrelation length scale  $L$  by considering multiple thermodynamic and dynamic factors and microphysical effects (e.g., precipitation) has the potential to improve the model-simulated total cloud covers.

In a recent study, Di Giuseppe and Tompkins (2015) applied the wind shear-dependent decorrelation length scale in the ECMWF Integrated Forecasting System. They found that the impact of wind shear-dependent parameterization on radiative budget calculation is comparable in magnitude to that of latitude-dependent scheme of Shonk et al. (2010). Our results also show that latitude-dependent scheme has similar bias of cloud cover relative to the new scheme developed in this study. Although our results can't suggest which of the scheme is superior, the scheme based on the meteorological factors has some potential advantages. For example, cloud overlap parameter is significantly controlled by atmospheric thermodynamic and dynamical conditions, therefore the long-term variations of meteorological factors are bound to affect the trend of cloud overlap and corresponding calculations of total cloud cover and radiation budget. Indeed, recent study has shown that rapid warming and an increase of atmospheric instability over the TP leads to more frequent deep clouds, which are responsible for the reduction of solar radiation over the TP (Yang et al., 2012). By using surface observations over 71 stations, some studies verified that annual and seasonal total cloud covers have declined during 1961-2005 (Duan and Wu, 2006; You et al., 2014). However, whether such variations of total cloud cover are linked with the changes of degree of cloud overlap over the TP are still unclear. Thus, more efforts are needed to reasonably evaluate the impact

of cloud overlap on the total cloud cover variations over these sensitive areas of climatic change (e.g., Tibetan Plateau and Arctic).

550 **Competing interests.** The authors declare that they have no conflict of interest.

**Acknowledgements.** This research was jointly supported by the key Program of the National Natural Science Foundation of China (41430425), the Foundation for Innovative Research Groups of the National Science Foundation of China (grant no. 41521004),  
555 National Science Foundation of China (grant nos. 41575015 and 41575143) and the China 111 project (grant no. B13045). We would like to thank the CALIPSO, CloudSat and ERA-Interim science teams for providing excellent and accessible data products that made this study possible. The CloudSat datasets are available from this link: (<http://www.cloudsat.cira.colostate.edu/order-data>), and ERA-Interim daily product may  
560 be accessed from (<http://apps.ecmwf.int/datasets/data/interim-full-daily/levtype=pl/>).

## References

- Barker, H. W., Stephens, G. L., and Fu, Q.: The sensitivity of domain-averaged solar fluxes to assumptions about cloud geometry, *Quart. J. R. Meteorol. Soc.*, 125, 2127-2152, 1999.
- 565 Barker, H.W., and Fu, Q.: Assessment and optimization of the Gamma-weighted two-stream approximation, *J. Atmos. Sci.*, 57, 1181-1188, 2000.
- Barker, H. W.: Overlap of fractional cloud for radiation calculations in GCMs: A global analysis using CloudSat and CALIPSO data, *J. Geophys. Res.*, 113(113), 762-770, 2008.
- Chang, F. L., and Li, Z.: A New Method for Detection of Cirrus Overlapping Water Clouds and  
570 Determination of Their Optical Properties, *J. Atmos. Sci.*, 62(11), 3993-4009, 2005a.
- Chang, F. L., and Li, Z.: A near global climatology of single-layer and overlapped clouds and their optical properties retrieved from TERRA/MODIS data using a new algorithm, *J. Clim.*, 18, 4752-4771, 2005b.
- Chen, B., and Liu, X.: Seasonal migration of cirrus clouds over the Asian Monsoon regions and the  
575 Tibetan Plateau measured from MODIS/Terra, *Geophys. Res. Lett.*, 32(320), 67-106, 2005.
- Chen, T., Rossow, W. B., and Zhang, Y.: Radiative Effects of Cloud-Type Variations, *J. Clim.*, 13, 264-286, 2000.
- Cheng, G. and Wu, T.: Responses of permafrost to climate change and their environmental significance, *Qinghai – Tibet Plateau, J. Geophys. Res.*, 112 (F2), F02S03, 2007.
- 580 Dee, D. P., Uppala, S. M., Simmons, A. J., Berrisford, P., Poli, P., Kobayashi, S., Andrae, U., Balmaseda, M., A. Balsamo, G., Bauer, P., Bechtold, P., Beljaars, A. C. M., Van De Berg, L.,

- Bidlot, J., Bormann, N., Delsol, C., Dragani, R., Fuentes, M., Geer, A., J. Haimberger, L., Healy, S. B., Hersbach, H., H $\ddot{o}$ m, E. V., Isaksen, I., K $\ddot{a}$ llberg, P., K $\ddot{o}$ hler, M., Matricardi, M., McNally, A. P., Monge-Sanz, B. M., Morcrette, J. J., Park, B. K., Peubey, C., De Rosnay, P., Tavolato, C., Th $\acute{e}$ aut, J. N., and Vitart, F.: The ERA-Interim reanalysis: configuration and performance of the data assimilation system, *Quart. J. R. Meteorol. Soc.*, 137(656), 553-597, 2011.
- 585 Di Giuseppe, F., and Tompkins, A. M.: Generalizing Cloud Overlap Treatment to Include the Effect of Wind Shear, *J. Atmos. Sci.*, 72, 2865-2876, 2015.
- Duan, A., and Xiao, Z.: Does the climate warming hiatus exist over the Tibetan Plateau?, *Scientific Reports*, 5, 13711, 2015.
- 590 Duan, A., and Wu, G.: Change of cloud amount and the climate warming on the Tibetan Plateau, *Geophys. Res. Lett.*, 33(22), 395-403, 2006.
- Duan, A. M., and Wu, G. X.: Role of the Tibetan Plateau thermal forcing in the summer climate patterns over subtropical Asia, *Clim. Dyn.*, 24(7), 793-807, 2005.
- 595 Fu, Q., and Liou, K. N.: Parameterization of the radiative properties of cirrus clouds, *J. Atmos. Sci.*, 50, 2008-2025, 1993.
- Fu, Q., Cribb, M.C., Barker, H.W., Krueger, S.K., and Grossman, A. 2000: Cloud geometry effects on atmospheric solar absorption, *J. Atmos. Sci.*, 57, 1156-1168, 2000;
- Fu, Q., Baker, M., and Hartmann, D.L.: Tropical cirrus and water vapor: An effective earth infrared iris feedback? *Atmos. Chem. Phys.*, 2, 1-7, 2002.
- 600 Fujinami, H., and Yasunari, T.: The seasonal and intraseasonal variability of diurnal cloud activity over the Tibetan Plateau, *J. Meteor. Soc. Japan*, 79, 1207-1227, 2001.
- Ge, J., Zhu, Z., Zheng, C., Xie, H., Zhou, T., Huang, J., and Fu, Q.: An improved hydrometeor detection method for millimeter-wavelength cloud radar, *Atmos. Chem. Phys.*, 17, 9035-9047, <https://doi.org/10.5194/acp-17-9035-2017>, 2017.
- 605 Ge, J., Zheng C., Xie, H., Xin Y., Huang J., and Fu Q.: Mid-latitude Cirrus Cloud at the SACOL site: Macrophysical Properties and Large-Scale Atmospheric State, *J. Geophys. Res.*, doi: 10.1002/2017JD027724, 2018
- Geleyn, J. F., and Hollingsworth, A.: An economical analytical method for the computation of the interaction between scattering and line absorption of radiation, *Contrib. Atmos. Phys.*, 52, 1-16, 1979.
- 610 Guo, D., and Wang, H.: The significant climate warming in the northern Tibetan Plateau and its possible causes, *Int. J. Climatol.*, 32, 1775 - 1781. <http://dx.doi.org/10.1002/joc.2388>, 2012.
- Haladay, T., and Stephens, G.: Characteristics of tropical thin cirrus clouds deduced from joint CloudSat and CALIPSO observations, *J. Geophys. Res.*, 114(114), D00A25-D00A37, 2009.
- 615 Hartmann, D. L., Ockert-Bell, M. E., and Michelsen, M. L.: The effect of cloud type on Earth's energy balance: Global analysis, *J. Clim.*, 5(11), 1281-1304, 1992.
- Hogan, R. J., and Illingworth, A. J.: Deriving cloud overlap statistics from radar, *Quart. J. R. Meteorol. Soc.*, 126(569), 2903-2909, 2000.
- 620 Huang, J. P., Minnis, P., and Lin, B.: Determination of ice water path in ice- over-water cloud systems using combined MODIS and AMSR-E measurements, *Geophys. Res. Lett.*, 33, L21801, doi:

10.1029/2006GL027038, 2006a.

Huang, J. P.: Analysis of ice water path retrieval errors over tropical ocean, *Adv. Atmos. Sci.*, 23, 165–180, 2006b.

625 Huang, J. P., Minnis, P., and Lin, B.: Advanced retrievals of multilayered cloud properties using multispectral measurements, *J. Geophys. Res.*, 110, D15S18, doi:10.1029/2004JD005101, 2005.

Jing, X., Zhang, H., Peng, J., Li, J., and Barker, H. W.: Cloud overlapping parameter obtained from CloudSat/CALIPSO dataset and its application in AGCM with McICA scheme, *Atmos. Res.*, 170, 52-65, 2016.

630 Kang, S., Xu, Y., You, Q., Flügel, W.A., Pepin, N. and Yao, T.: Review of climate and cryospheric change in the Tibetan Plateau, *Environ. Res. Lett.*, 5, 015101.<http://dx.doi.org/10.1088/1748-9326/5/1/015101>, 2010.

Kato, S., Sun-Mack, S., Miller, W. F., Rose, F. G., Chen, Y., Minnis, P., and Wielicki, B. A.: Relationships among cloud occurrence frequency, overlap, and effective thickness derived from  
635 CALIPSO and CloudSat merged cloud vertical profiles, *J. Geophys. Res.*, 115(D4), 1-28, 2010.

Kawamoto, K. and Suzuki, K.: Microphysical transition in water clouds Over the Amazon and China derived from spaceborne radar and Radiometer data, *J. Geophys. Res.*, 117, D05212, doi:10.1029/2011JD016412, 2012.

Li, J., Huang, J., Stamnes, K., Wang, T., Lv, Q., and Jin, H.: A global survey of cloud overlap based  
640 on CALIPSO and CloudSat measurements, *Atmos. Chem. Phys.*, 15(1), 519-536, 2015.

Li, J., Hu, Y., Huang, J., Stamnes, K., Yi, Y., and Stamnes, S.: A new method for retrieval of the extinction coefficient of water clouds by using the tail of the CALIOP signal, *Atmos. Chem. Phys.*, 11(6), 2903-2916, 2011.

Li, J., Yi, Y., Minnis, P., Huang, J., Yan, H., Ma, Y., Wang, W., and Ayers, K.: Radiative effect  
645 differences between multi-layered and single-layer clouds derived from CERES, CALIPSO, and CloudSat data, *J. Quant. Spectrosc. Radiat. Transf.*, 112, 361-375, 2011.

Li, Y., Liu, X., and Chen B.: Cloud type climatology over the Tibetan Plateau: A comparison of ISCCP and MODIS/TERRA measurements with surface observations, *Geophys. Res. Lett.*, 33, L17716, doi:10.1029/2006GL026890, 2006.

650 Li, Y. Y., and Zhang, M.: Cumulus over the Tibetan Plateau in the summer based on CloudSat–CALIPSO data, *J. Climate*, 29, 1219–1230, doi:10.1175/JCLI-D-15-0492.1, 2016.

Mace, G. G., and Zhang, Q.: The CloudSat radar-lidar geometrical profile product (RL-GeoProf): Updates, improvements, and selected results, *J. Geophys. Res.*, 119(15), 9441-9462, doi:10.1002/2013JD021374, 2014.

655 Mace, G. G., Zhang, Q., Vaughan, M., Marchand, R., Stephens, G., Trepte, C., and Winker, D.: A description of hydrometeor layer occurrence statistics derived from the first year of merged CloudSat and CALIPSO data, *J. Geophys. Res.*, 114, D00A26, doi:10.1029/2007JD009755, 2009.

Mace, G. G., and Bensonroth, S.: Cloud-Layer Overlap Characteristics Derived from Long-Term  
660 Cloud Radar Data, *J. Clim.*, 15(17), 2505-2515, 2002.

Morcrette, J. J., and Jakob, C.: The response of the ECMWF model to changes in the cloud overlap

- assumption, *Mon. Wea. Rev.*, 128, 1707–1732, 2000.
- Morcrette, J. J., and Fouquart, Y.: The Overlapping of Cloud Layers in Shortwave Radiation Parameterizations, *J. Atmos. Sci.*, 43(4),321-328, 1986.
- 665 Naud, C. M., Del Genio, A., Mace, G. G., Benson, S., Clothiaux, E. E., and Kollias, P.: Impact of dynamics and atmospheric state on cloud vertical overlap, *J. Clim.*, 21(8), 1758-1770, 2008.
- Oreopoulos, L., and Norris, P. M.: An analysis of cloud overlap at a midlatitude atmospheric observation facility, *Atmos. Chem. Phys.*, 11(1), 5557-5567, 2011.
- Oreopoulos, L., and Khairoutdinov, M.: Overlap properties of clouds generated by a cloud-resolving  
670 model, *J. Geophys. Res.*, 108, 4479, doi:10.1029/2002JD003329, 2003.
- Pincus, R., Hannay, C., Klein, S. A., Xu, K. M., and Hemler, R.: Overlap assumptions for assumed probability distribution function cloud schemes in large-scale models, *J. Geophys. Res.*, 110(D15), 2005.
- Shonk, J. K. P., Hogan, R. J., and Manners, J.: Impact of improved representation of horizontal and  
675 vertical cloud structure in a climate model, *Clim. Dyn.*, 38, 2365-2376, 2014.
- Shonk, J. K., Hogan, R. J., Edwards, J. M., and Mace, G. G.: Effect of improving representation of horizontal and vertical cloud structure on the Earth's global radiation budget. Part I: Review and parametrization, *Quart. J. R. Meteorol. Soc.*, 136(650), 1191-1204, 2010.
- Stephens, G. L., Vane, D. G., Boain, R. J., Mace, G. G., Sassen, K., Wang, Z., Illingworth, A. J.,  
680 O'Connor, E. J., Rossow, W. B., Durden, S. L., Miller, S. D., Austin, R. T., Benedetti, A., Mitrescu, C., and CloudSat Science Team.: The CloudSat mission and the A-Train, A new dimension of space-based observations of clouds and precipitation, *B. Am. Meteor. Soc.*, 83, 1771-1790, 2002.
- Taniguchi, K., and Koike, T.: Seasonal variation of cloud activity and atmospheric profiles over the  
685 eastern part of the Tibetan Plateau. *J. Geophys. Res.*, 113(D10), 523-531, 2008.
- Tompkins, A., and Giuseppe, F. D.: An interpretation of cloud overlap statistics, *J. Atmos. Sci.*, 72, 2877-2889, 2015.
- Verlinden, K. L., Thompson, D. W. J., and Stephens, G. L.: The Three-Dimensional Distribution of  
Clouds over the Southern Hemisphere High Latitudes, *J. Clim.*, 24(24), 5799-5811, 2011.
- 690 Wang, B., Bao, Q., Hoskins, B., Wu, G. and Liu, Y.: Tibetan Plateau warming and precipitation changes in East Asia, *Geophys. Res. Lett.*, 35, L14702, 2008
- Wang, M. Y., Gu, J., Yang, R., Zeng, L. and Wang, S.: Comparison of cloud type and frequency over China from surface, FY-2E, and CloudSat observations. *Remote Sensing of the Atmosphere, Clouds, and Precipitation*, E. Im, S. Yang, and P. Zhang, Eds., International Society for Optical  
695 Engineering(SPIE Proceedings, Vol. 9259), doi:10.1117/12.2069110, 2014.
- Wang, W., Huang, J., Minnis, P., Hu, Y., Li, J., Huang, Z., Ayers, J. K., and Wang, T.: Dusty cloud properties and radiative forcing over dust source and downwind regions derived from A-Train data during the Pacific Dust Experiment, *J. Geophys. Res.*, 115, D00H35, doi:10.1029/2010JD014109, 2010.
- 700 Weger, R. C., Lee, J., Zhu, T., and Welch, R. M.: Clustering, randomness and regularity in cloud fields: 1. Theoretical considerations, *J. Geophys. Res.*, 97, 20519–20536, doi:10.1029/92JD02038,

1992.

- Willén, U., Crewell, S., Baltink, H. K., and Sievers, O.: Assessing model predicted vertical cloud structure and cloud overlap with radar and lidar ceilometer observations for the Baltex Bridge  
705 Campaign of CLIWA-NET, *Atmos. Res.*, 75(3), 227-255, 2005.
- Winker, D. M., Hunt, W. H. and McGill, M. J.: Initial performance assessment of CALIOP, *Geophys. Res. Lett.*, 34(19), 228-262, 2007.
- Wu, G., Duan, A., Liu, Y., Mao, J., Ren, R., Bao, Q., He, B., Liu, B., and Hu, W.: Tibetan Plateau climate dynamics: recent research progress and outlook, *National Science Review*, 2(1), 100-116,  
710 2015.
- Wu, G. X., Liu, Y., Wang, T., Wan, R., Liu, X., Li, W., Wang, Z., Zhang, Q., Duan, A., and Liang X.: The influence of the mechanical and thermal forcing of the Tibetan Plateau on the Asian climate, *J. Hydrometeorol.*, 8, 770–789, doi:10.1175/JHM609.1, 2007.
- Wu, H., Yang, K., Niu, X., and Chen, Y.: The role of cloud height and warming in the decadal  
715 weakening of atmospheric heat source over the Tibetan Plateau, *Sci. China Ser. D.*, 58(3), 395–403, doi:10.1007/s11430-014-4973-6, 2015.
- Xu, X., Lu, C., Shi, X., and Gao, S.: World water tower: An atmospheric perspective, *Geophys. Res. Lett.*, 35(20), 525-530, 2008.
- Yan, H.R., Li, Z.Q., Huang, J.P., Cribb, M., Liu, J.J.: Long-term aerosol-mediated changes in cloud  
720 radiative forcing of deep clouds at the top and bottom of the atmosphere over the Southern Great Plains, *Atmos. Chem. Phys.*, 14(14), 7113-7124, 2014.
- Yan, Y., Liu, Y. and Lu, J.: Cloud vertical structure, precipitation, and cloud radiative effects over Tibetan Plateau and its neighboring regions, *J. Geophys. Res. Atmos.*, 121(2016), pp.5864-5877, 10.1002/2015JD024591, 2016.
- 725 Yanai, M., Li, C. F., and Song, Z. S.: Seasonal heating of the Tibetan Plateau and its effects on the evolution of the Asian summer monsoon, *J. Meteor. Soc. Japan*, 70, 319–351, 1992.
- Yang, K., Wu, H., Qin, J., Lin, C., Tang, W., and Chen, Y.: Recent climate changes over the Tibetan Plateau and their impacts on energy and water cycle: A review, *Global and Planetary Change*, 112(1), 79-91, 2014.
- 730 Yang, K., Ding B., Qin, J., Tang W., Lu, N., and Lin, C.: Can aerosol loading explain the solar dimming over the Tibetan Plateau?, *Geophys. Res. Lett.*, 39, L20710, doi: 10.1029/2012GL053733, 2012.
- Yang, K., Guo, X., He, J., Qin, J. and Koike, T.: On the climatology and trend of the atmospheric heat source over the Tibetan Plateau: an experiments-supported revisit, *J. Clim.*, 24, 1525 – 1541,  
735 2011.
- Yoo, H., Li, Z., You, Y., Lord, S., Weng F, and Barker H. W.: Diagnosis and testing of low-level cloud parameterizations for the NCEP/GFS model satellite and ground-based measurements, *Clim. Dyn.*, 41(5-6), 1595-1613, doi:10.1007/s00382-013-1884-8, 2013.
- 740 You, Q., Jiao, Y., Lin, H., Min, J., Kang, S., Ren, G., and Meng, X.: Comparison of NCEP/NCAR and ERA-40 total cloud cover with surface observations over the Tibetan Plateau, *International Journal of Climatology*, 34(8), 2529-2537, 2014.

Yuan, T., and Oreopoulos, L.: On the global character of overlap between low and high clouds, *Geophys. Res. Lett.*, 40, 5320-5326, 2013.

Zhang, H., and Jing, X.: Advances in studies of cloud overlap and its radiative transfer in climate models, *J. Meteorol. Res.*, 30(2), 156-168, 2016.

Zhang, H., Peng, J., Jing, X., and Li, J.: The features of cloud overlapping in Eastern Asia and their effect on cloud radiative forcing, *Science China Earth Sciences*, 56(5), 737-747, 2013.

Zhang, H., and Jing, X. W.: Effect of cloud overlap assumptions in climate models on modeled earth-atmosphere radiative fields, *Chinese Journal of Atmospheric Sciences*, 34(3), 520-532, 2010.

Zhao, C.F., Liu, L.P., Wang, Q.Q., Qiu, Y.M., Wang, Y., and Wu, X. L.: MMCR-based characteristic properties of non-precipitating cloud liquid droplets at Naqu site over Tibetan Plateau in July 2014, *Atmospheric research*, 190, 68-76, doi.org/10.1016/j.atmosres.2017.02.002, 2017.

Zhao, C.F., Liu, L.P., Wang, Q.Q., Qiu, Y.M., Wang, W., Wang, Y., and Fan, T.Y.: Toward Understanding the Properties of High Ice Clouds at the Naqu Site on the Tibetan Plateau Using Ground-Based Active Remote Sensing Measurements Obtained during a Short Period in July 2014, *Journal of Applied Meteorology and Climatology*, 55, 2493-2507, doi:10.1175/JAMC-D-16-0038.1, 2016.

Zhu, L., Xie, M. and Wu, Y.: Quantitative analysis of lake area variations and the influence factors from 1971 to 2004 in the Nam Co basin of the Tibetan Plateau, *Chin. Sci. Bull.* 55, 1294 - 1303, 2010.

Table 1. Parameterizations of decorrelation scale length  $L$  from the exponential fit as a function of atmospheric stability  $\partial\theta_{es}/\partial z$ , wind shear  $dV/dz$  or latitude  $\Phi$

Scheme	description	decorrelation length scale $L$
Wind shear (Di Giuseppe and Tompkins, 2015)	Random/Maximum, only wind shear	$L = 4.4 - 0.45 \times \frac{dV}{dz}$
Wind shear (this study)	Random/Maximum, only wind shear	$L = 2.19 - 0.14 \times \frac{dV}{dz}$
Wind shear-instability (this study)	Random/Maximum, wind shear and instability	$L = 2.18 - 0.09 \times \frac{dV}{dz} - 0.15 \times \frac{\partial\theta_{es}}{dz}$
Latitude (Shonk et al., 2010)	Random/Maximum, only latitude	$L = 2.899 - 0.02759 \times  \Phi $



## Figure Captions

**Figure 1.** (a) CloudSat overpass tracks (blue line: daytime; red line: nighttime) over the Tibetan Plateau (27°N-39°N; 78°E-103°E); (b) A sample of CloudSat  
775 2B-GEOPROF-LIDAR cloud mask product along the ground track of 200km (white color: cloud fraction > 99%; light blue: 0 < cloud fraction < 99%; deep blue: clear sky; orange color: surface). (c) The observed and calculated segment-average cloud cover profiles based on maximum and random assumptions for different spatial scales and given cloud mask sample in Fig. 1b. (d) The corresponding cloud overlap parameters of  
780 contiguous cloud layers for 25, 50, 100 and 200 km spatial scales, respectively. Note that the observations below 1 km over the TP surface have been removed.

**Figure 2.** The dependence of  $\alpha$  on the layer separation and its sensitivity to the spatial  
785 scale for (a) noncontiguous and (b) contiguous cloud pairs; the error bars correspond to  $\pm 3$  standard error; (c) The probability distribution functions (PDFs) of the along-track horizontal scales of cloud system at different height over TP region; (d) The variations of cloud sample number and the cumulative percentages with cloud layer separations for both noncontiguous and contiguous clouds at a given spatial scale of 50km. The  
790 cumulative percentages represent the proportions of cloud sample below corresponding layer separation to all samples.

**Figure 3.** The monthly variations of the pentad-averaged (a) cloud overlap parameter,  $\alpha$ ,  
795 (c) conditional instability to moist convection,  $\partial\theta_{es}/\partial z$ , (e) wind shear,  $dV/dz$ , (g) and vertical velocity at 500 hPa,  $\omega$  for the contiguous cloud layers over the TP; The monthly variations of the pentad-averaged (b)  $\alpha$ , (d)  $\partial\theta_{es}/\partial z$ , (f)  $dV/dz$  and (h)  $\omega$  for the contiguous clouds for the layer separation of 2 km (red) and 3km (black).

**Figure 4.** The zonal variations of the (a)  $\alpha$ , (c)  $\partial\theta_{es}/\partial z$ , (e)  $dV/dz$ , and (g)  $\omega$  for the  
800 contiguous cloud layers over the TP; The zonal variations of the (b)  $\alpha$ , (d)  $\partial\theta_{es}/\partial z$ , (f)  $dV/dz$  and (h)  $\omega$  for the contiguous cloud layers for the layer separation of 2 km (red) and 3km (black).

**Figure 5.** The sensitivities of median overlap parameter  $\alpha$  to the (a) wind shear, (b)  
805 instability and (c) vertical velocity at 500 hPa at given upper limit of cloud cover (50%)

and spatial scale (50 km) for the contiguous cloud layers. The error bars correspond to  $\pm 3$  standard error.

**Figure 6.** The monthly differences in total cloud cover between calculation and observation for different schemes (see the Table 1) and its dependence on the layer separation.

**Figure 7.** The zonal differences in cloud cover between calculation and observation for different schemes (see the Table 1) and its dependence on the layer separation.

815

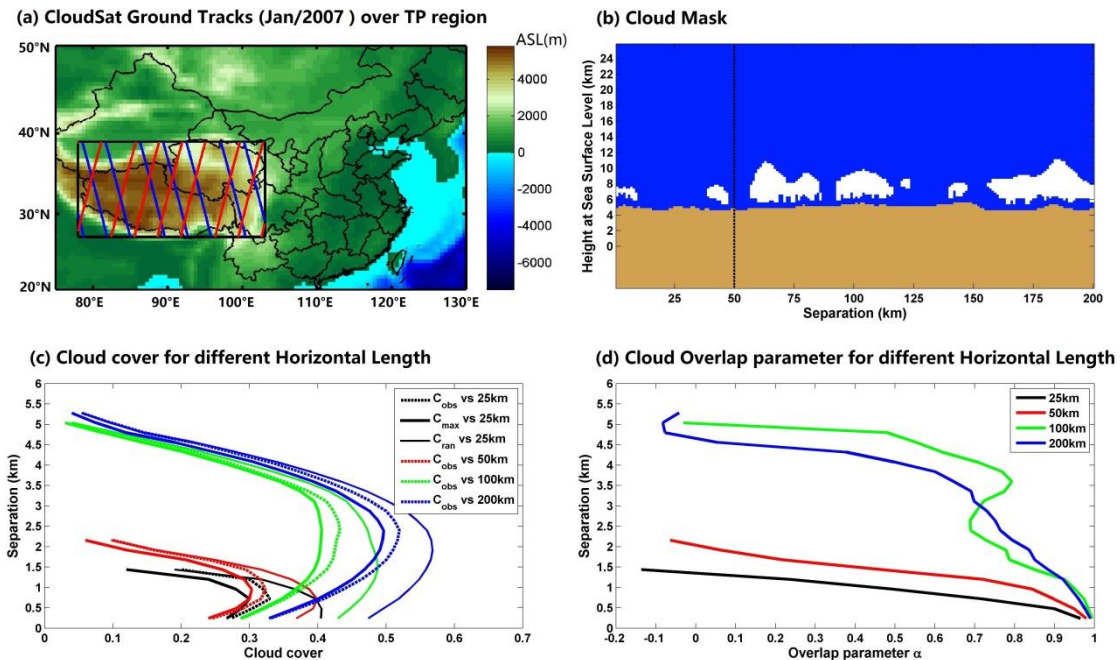


**Figure 1.** (a) CloudSat overpass tracks (blue line: daytime; red line: nighttime) over the Tibetan Plateau (27 N-39 N; 78 E-103 E); (b) A sample of CloudSat 2B-GEOPROF-LIDAR cloud mask product along the ground track of 200km (white color: cloud fraction > 99%; light blue: 0 < cloud fraction < 99%; deep blue: clear sky; orange color: surface). (c) The observed and calculated segment-average cloud cover profiles based on maximum and random assumptions for different spatial scales and given cloud mask sample in Fig. 1b. (d) The corresponding cloud overlap parameters of

825

contiguous cloud layers for 25, 50, 100 and 200 km spatial scales, respectively. Note that the observations below 1 km over the TP surface have been removed.

830

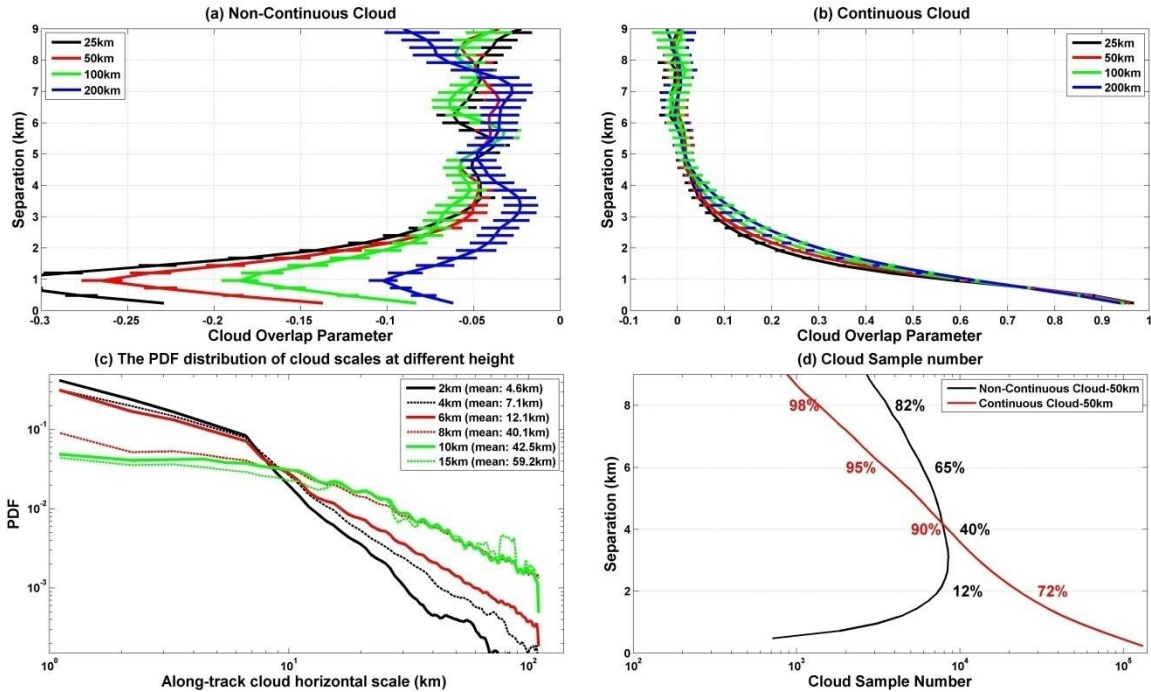


**Figure 2.** The dependence of  $\alpha$  on the layer separation and its sensitivity to the spatial scale for (a) noncontiguous and (b) contiguous cloud pairs; the error bars correspond to  $\pm 3$  standard error; (c) The probability distribution functions (PDFs) of the along-track horizontal scales of cloud system at different height over TP region; (d) The variations of cloud sample number and the cumulative percentages with cloud layer separations for both noncontiguous and contiguous clouds at a given spatial scale of 50km. The cumulative percentages represent the proportions of cloud sample below corresponding layer separation to all samples.

840

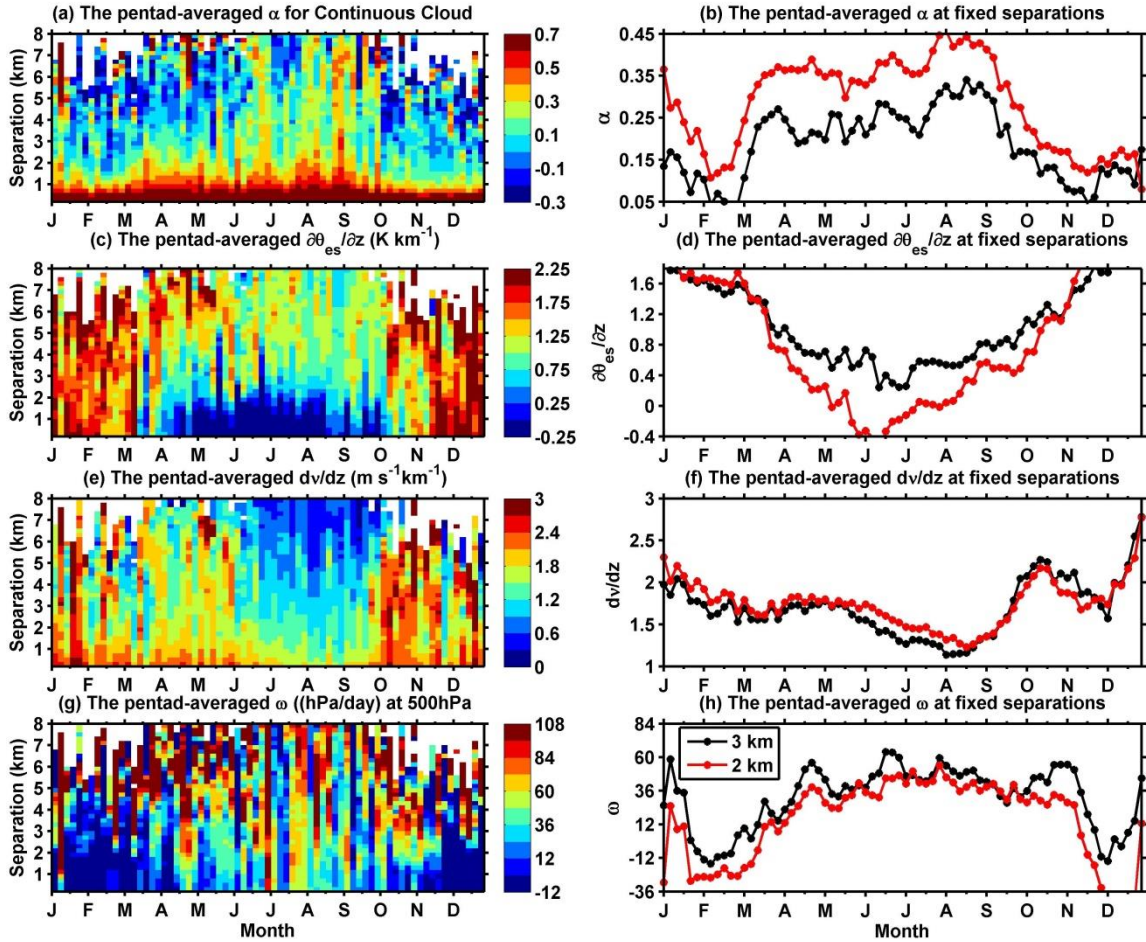


**Figure 3.** The monthly variations of the pentad-averaged (a) cloud overlap parameter,  $\alpha$ , (c) conditional instability to moist convection,  $\partial\theta_{es}/\partial z$ , (e) wind shear,  $dV/dz$ , (g) and vertical velocity at 500 hPa,  $\omega$  for the contiguous cloud layers over the TP ; The monthly variations of the pentad-averaged (b)  $\alpha$ , (d)  $\partial\theta_{es}/\partial z$ , (f)  $dV/dz$  and (h)  $\omega$  for the contiguous clouds for the layer separation of 2 km (red) and 3km (black).

845

850

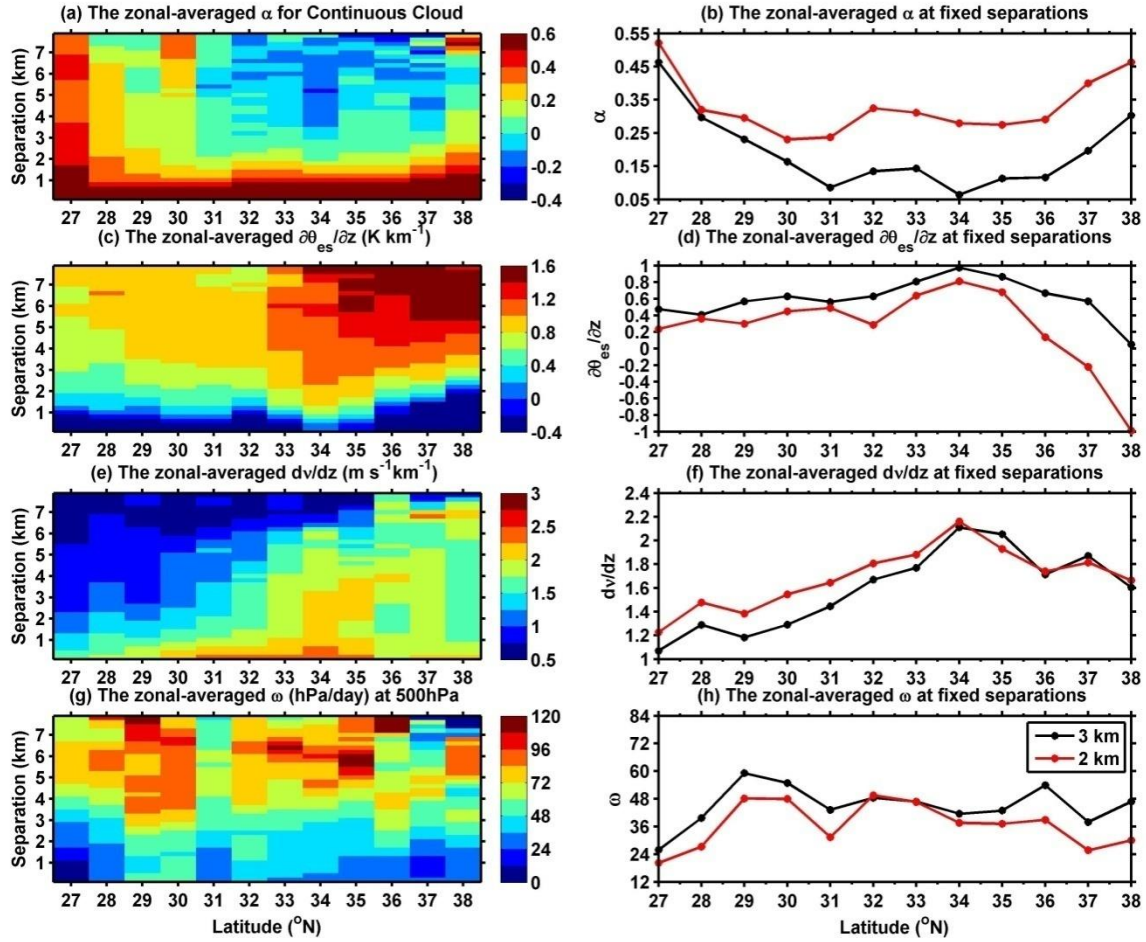
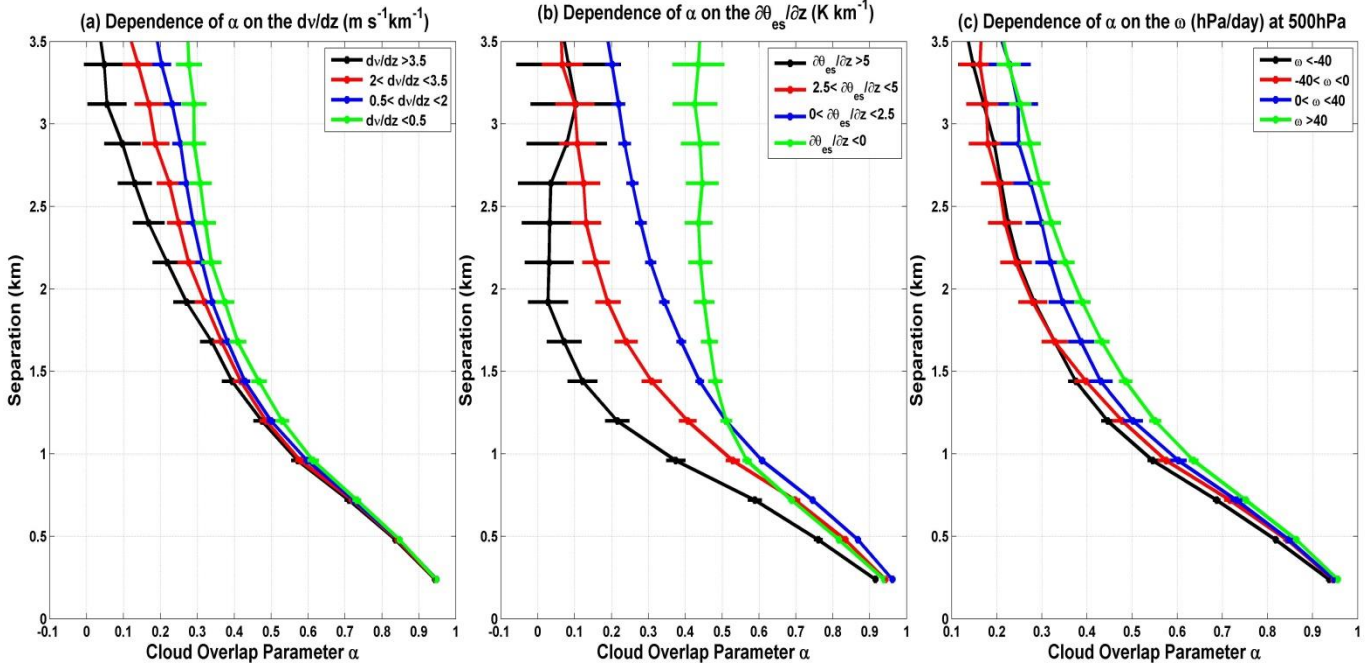


**Figure 4.** The zonal variations of the (a)  $\alpha$ , (c)  $\partial\theta_{es}/\partial z$ , (e)  $dV/dz$ , and (g)  $\omega$  for the contiguous cloud layers over the TP; The zonal variations of the (b)  $\alpha$ , (d)  $\partial\theta_{es}/\partial z$ , (f)  $dV/dz$  and (h)  $\omega$  for the contiguous cloud layers for the layer separation of 2 km (red) and 3km (black).

855

860



865

**Figure 5.** The sensitivities of median overlap parameter  $\alpha$  to the (a) wind shear, (b) instability and (c) vertical velocity at 500 hPa at given upper limit of cloud cover (50%) and spatial scale (50 km) for the contiguous cloud layers. The error bars correspond to  $\pm 3$  standard error.

870

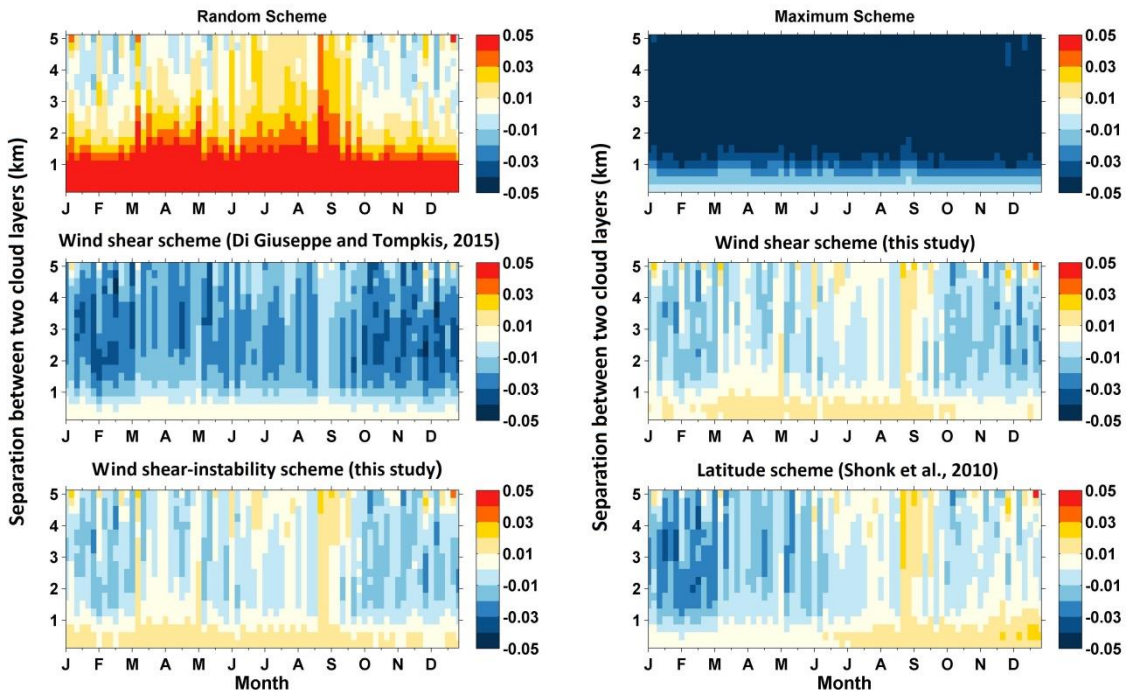


Figure 6. The monthly differences in cloud cover between calculation and observation for different schemes (see the Table 1) and its dependence on the layer separation.

875

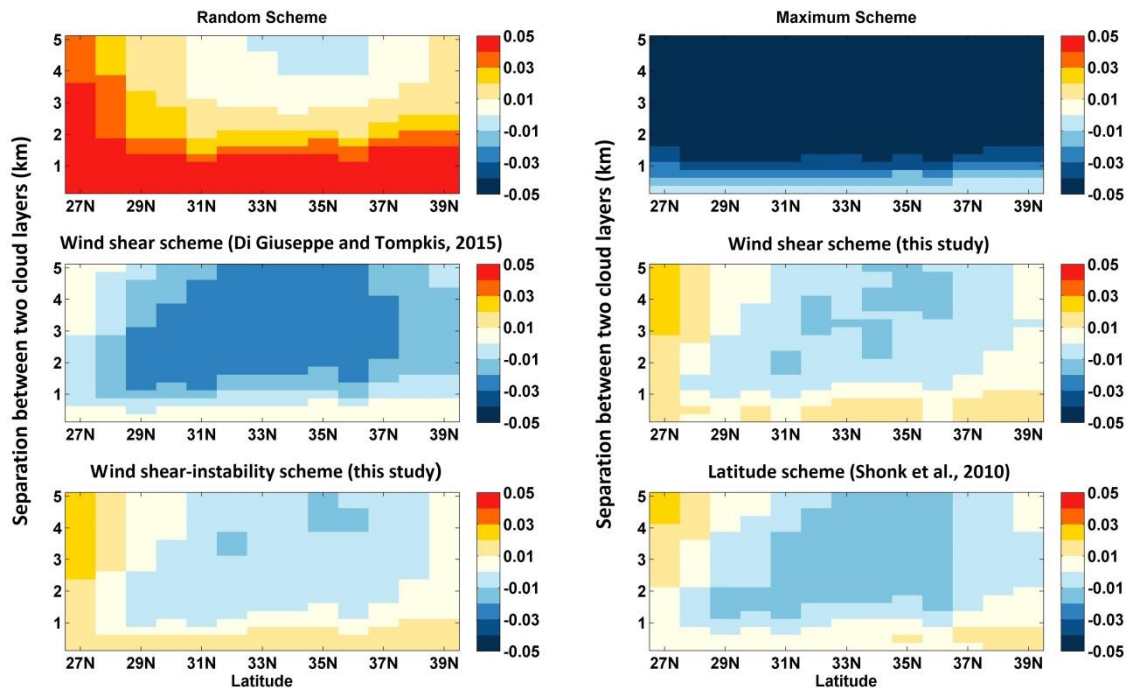


Figure 7. The zonal differences in cloud cover between calculation and observation for different schemes (see the Table 1) and its dependence on the layer separation.

880